





# Getting the phase consistent: The importance of phase description in balanced steady-state free precession MRI of multi-compartment systems

Nils M. J. Plähn<sup>1,2,3</sup>  | Simone Poli<sup>2,3,4</sup> | Eva S. Peper<sup>1,2</sup> | Berk C. Açikgöz<sup>1,2,3</sup> | Roland Kreis<sup>2,4,5</sup>  | Carl Ganter<sup>6</sup>  | Jessica A. M. Bastiaansen<sup>1,2</sup> 

<sup>1</sup>Department of Diagnostic, Interventional and Pediatric Radiology (DIPR), Inselspital, Bern University Hospital, University of Bern, Bern, Switzerland

<sup>2</sup>Translation Imaging Center (TIC), Swiss Institute for Translational and Entrepreneurial Medicine, Bern, Switzerland

<sup>3</sup>Graduate School for Cellular and Biomedical Sciences, University of Bern, Bern, Switzerland

<sup>4</sup>MR Methodology, Department for Diagnostic and Interventional Neuroradiology, University of Bern, Bern, Switzerland

<sup>5</sup>Department for Biomedical Research, University of Bern, Bern, Switzerland

<sup>6</sup>Department of Diagnostic and Interventional Radiology, TUM School of Medicine and Health, Klinikum rechts der Isar, Technical University of Munich, Munich, Germany

## Correspondence

Jessica A. M. Bastiaansen, Department of Diagnostic, Interventional and Pediatric Radiology (DIPR), Inselspital, Bern University Hospital, University of Bern, Bern, Switzerland.  
Email: [jbastiaansen.mri@gmail.com](mailto:jbastiaansen.mri@gmail.com)

## Funding information

Swiss National Science Foundation, Grant/Award Number: PCEFP2\_194296

## Abstract

**Purpose:** Determine the correct mathematical phase description for balanced steady-state free precession (bSSFP) signals in multi-compartment systems.

**Theory and Methods:** Based on published bSSFP signal models, different phase descriptions can be formulated: one predicting the presence and the other predicting the absence of destructive interference effects in multi-compartment systems. Numerical simulations of bSSFP signals of water and acetone were performed to evaluate the predictions of these different phase descriptions. For experimental validation, bSSFP profiles were measured at 3T using phase-cycled bSSFP acquisitions performed in a phantom containing mixtures of water and acetone, which replicates a system with two signal components. Localized single voxel MRS was performed at 7T to determine the relative chemical shift of the acetone-water mixtures.

**Results:** Based on the choice of phase description, the simulated bSSFP profiles of water-acetone mixtures varied significantly, either displaying or lacking destructive interference effects, as predicted theoretically. In phantom experiments, destructive interference was consistently observed in the measured bSSFP profiles of water-acetone mixtures, supporting the theoretical description that predicts such interference effects. The connection between the choice of phase description and predicted observation enables unambiguous experimental identification of the correct phase description for multi-compartment bSSFP profiles, which is consistent with the Bloch equations.

**Conclusion:** The study emphasizes that consistent phase descriptions are crucial for accurately describing multi-compartment bSSFP signals, as incorrect phase descriptions result in erroneous predictions.

## KEYWORDS

asymmetries, balanced steady-state free precession, multi-compartment, phase definition, phase-cycled bSSFP, signal model

## 1 | INTRODUCTION

Balanced steady-state free precession (bSSFP) MRI sequences provide images with a high SNR and  $T_2/T_1$  contrast.<sup>1</sup> Phase-cycled bSSFP, which refers to multiple MRI acquisitions with different linear phase increments of the RF excitation pulse, can be used for banding artifact removal,<sup>2–8</sup> the quantification of the  $T_1$  and  $T_2$  relaxation times,<sup>9–13</sup> and the quantification of fat fraction within a voxel.<sup>14</sup> The complex signal as a function of the RF phase increment is usually known as a “bSSFP profile.” For banding artifact removal techniques such as geometric solution,<sup>8</sup> as well as for multi-parameter quantification,<sup>9–13</sup> the signal phase of the bSSFP profile is a crucial source of information.<sup>8–10</sup>

In addition to previous studies on water-fat fraction mapping,<sup>14</sup> most quantitative mapping methods using bSSFP profiles<sup>9–13</sup> typically assume that a voxel has a single compartment with a distinct resonance frequency. In such scenarios, the bSSFP profile appears elliptical on a complex plane, exhibiting axial symmetry with respect to the off-resonance value when plotted as a function of the RF phase increment. While the complex bSSFP profile has been extensively characterized for single-compartment systems,<sup>2,9–12,15–19</sup> showcasing a symmetric and elliptical shape, deviations from symmetry emerge in the presence of gray matter, white matter, and muscle,<sup>9,20,21</sup> as well as in voxels containing multiple resonance frequencies, such as water and fat.<sup>14</sup> Although descriptions for bSSFP profiles in multi-compartment systems have been reported<sup>11</sup> their examination and validation regarding asymmetric signal behavior remain limited.

Because certain elements of bSSFP signal phase descriptions may affect how two single component profiles are superimposed, the study aimed to determine the correct mathematical phase description for multi-compartment bSSFP profiles. An intuitive derivation and experimental validation are provided using water acetone mixtures. Acetone was selected over fat due to its improved solubility, and to mimic a scenario with two distinct signal components.

## 2 | THEORY

In bSSFP, a near zero signal is observed when the RF phase increment ( $\varphi$ ) balances the local off-resonance-induced phase accumulated ( $\vartheta$ ) between two successive RF excitation pulses.<sup>1</sup> This near-zero signal is responsible for the commonly observed banding artifacts in bSSFP. In multi-compartment systems, asymmetric profiles were suggested to originate from convolution between the

local frequency distribution and a bSSFP profile.<sup>20,21</sup> Therefore, the final combined profile is an integration of all off-resonant profiles within a voxel, which can be understood using the superposition principle. It can be argued that a near-zero signal obtained with a specific RF phase increment might be the consequence of superposition rather than off-resonance, arising from destructive interference of signals from different tissue types, such as water and fat, within the same imaging voxel. This section aims to describe the destructive interference behavior of bSSFP in multi-compartment systems with distinct signal components.

### 2.1 | Phase-cycled bSSFP signal model

The signal equation of the magnetization  $m_+$  at time  $t = 0^+$  directly after the RF excitation pulse of a bSSFP sequence can be written<sup>2,17,19</sup> in the rotating coordinate frame as

$$m_+(0^+, \varphi) = e^{i\psi} \frac{a}{b + c \cos(\vartheta - \varphi)} (1 - E_2 e^{-i(\vartheta - \varphi)}) \quad (1)$$

with  $\varphi$  the RF phase increment and  $\vartheta$  the *accumulated phase* as defined in,<sup>17</sup> which is a phase directly proportional to local off-resonance that is, chemical shift  $\delta_{cs}$  and magnetic field inhomogeneity  $\Delta B_0$ . The constants of Eq. (1) are defined<sup>2,17,19</sup> as  $a = KM_0(1 - E_1) \sin(\alpha)$ ,  $b = 1 - E_1 E_2^2 + (E_2^2 - E_1) \cos(\alpha)$  and  $c = (E_1 - 1)E_2(\cos(\alpha) + 1)$ . The (usually unknown) phase factor  $e^{i\psi}$  depends on combined effects, such as the chosen RF rotation axis (in the rotating frame), local coil phases, receiver offsets or postprocessing (coil combination, phase regularization), but is constant over time if no phase drift (e.g.,  $B_0$ -drift) occurs.<sup>12</sup>  $K$  is the magnitude of the combined receiver field and depends on local coil sensitivities.  $E_i = \exp\left(\frac{-TR}{T_i}\right)$  is the relaxation term describing the longitudinal ( $T_1$ ) and transverse ( $T_2$ ) relaxation time ( $i = 1, 2$ ) with repetition time TR, RF excitation angle  $\alpha$ , and the thermal equilibrium magnetization  $M_0$ . Unless specified, the magnetization  $m_+$  is represented in right-handed coordinate systems which can be realized without loss of generality via

$$m_+ = M_x + i \cdot M_y. \quad (2)$$

Switching between left- and right- handed coordinate systems can be achieved by complex conjugation of Eq. (2). Switching the handedness of the coordinate system leads to inverted signs of the phases in Eqs. (1, 3, 4) and to two different phase settings:  $\cos(x) \pm i \cdot \sin(x) = e^{\pm ix}$ .

## 2.2 | Definition of accumulated phase and phase evolution

Using the accumulated phase definition  $\vartheta$ , the phase evolution for bSSFP signals at timepoint  $t$  can be described as:

$$m_+(t, \varphi) = e^{i\frac{t}{TR}\vartheta} \cdot e^{-\frac{t}{T_2}} \cdot m_+(0^+, \varphi). \quad (3)$$

To identify the accumulated phase, Eq. (3) can be compared with the solution of the Bloch equation<sup>22</sup>

$$m_+(t, \varphi) = e^{-iyB_0t} \cdot e^{-\frac{t}{T_2}} \cdot m_+(0^+, \varphi) \quad (4)$$

with the main magnetic field  $B_0$  and for positive gyromagnetic ratios  $\gamma$ .<sup>23</sup> In rotating coordinate frames, only residual magnetic field inhomogeneity remains. Therefore, in the case of isochromatic spin systems,  $B_0$  in Eq. (4) can be substituted by  $B_0 \rightarrow \Delta B_0$ . When dealing with multiple types of isochromatic spins in a system, each associated with different chemical shifts<sup>25</sup>  $\delta_{cs}$ ,  $B_0$  can be substituted by  $B_0 \rightarrow (\Delta B_0 + \delta_{cs}B_0)$ .<sup>16,24</sup> Combining Eqs. (3, 4) allows the determination of the accumulated phase

$$\vartheta = -\gamma(\Delta B_0 + \delta_{cs}B_0)TR. \quad (5)$$

At this point, a first look at phases and their respective signs can be performed:

- While the minus sign in Eq. (5) follows from the solution of the Bloch equation (Eq. 4), reconstructed MRI data does not necessarily rely on that convention. This merely reflects a choice regarding the handedness of the underlying coordinate system.
- Regardless of the chosen coordinate system, the steady state in Eq. (1) must depend on the *difference* between the accumulated phase  $\vartheta$  and RF phase increment  $\varphi$ , since changing both by the same amount must not modulate the steady-state amplitude.
- At  $TE = TR/2$ , the phase-related terms in Eqs. (1, 3) combine (in addition to small corrections of order  $O(1 - E_2)$ ) to

$$2i e^{i\varphi/2} \cdot \sin \frac{\vartheta - \varphi}{2} \quad (6)$$

- Since  $e^{i\vartheta/2} \cdot (1 - e^{-i(\vartheta-\varphi)}) = e^{i\varphi/2} \cdot (e^{i(\vartheta-\varphi)/2} - e^{-i(\vartheta-\varphi)/2}) = 2i e^{i\varphi/2} \cdot \sin \frac{\vartheta-\varphi}{2}$ . (see Theory S1 for a more detailed derivation). Apart from banding artifacts occurring at  $\vartheta \approx \varphi + n \cdot 2\pi$  (independent of the echo time), this term (Eq. 6) reflects some of the fundamental properties of bSSFP at  $TE = TR/2$ :

- a. The steady state is  $4\pi$ -periodic with respect to  $\vartheta$ .

- b. The signal phase, as a function of  $\vartheta - \varphi$ , is essentially constant ( $\approx \varphi/2 + n \cdot \pi + \psi + \pi/2$ ) within any bSSFP plateau (numbered by  $n$ ) between two subsequent banding artifacts (see also Eq. 9 below). This is also consistent with the well-known spin-echo-like behavior of bSSFP<sup>25</sup> for moderate field inhomogeneity.

Property (b) no longer holds if the phase evolution in Eq. (3) is replaced by its complex conjugate  $e^{-i\frac{t}{TR}\vartheta}$ , since at  $TE = TR/2$  this would correspond to a multiplication with  $e^{-i\frac{\vartheta}{2}}$  instead of  $e^{i\frac{\vartheta}{2}}$ , such that the phase-related term in Eq. (3) combine to

$$2i e^{-i\vartheta} \cdot e^{i\varphi/2} \cdot \sin \frac{\vartheta - \varphi}{2} \quad (7)$$

(see Theory S2 for a more detailed derivation). For a single isochromat with some fixed (and unknown)  $\vartheta$ , this particular combination of steady state and phase evolution should not be noticeable since the factor  $e^{-i\vartheta}$  would be absorbed in the unknown factor  $e^{i\psi}$  in Eq. (1). Which, more intuitively, means that, for both instances (Eqs. 6 or 7), the shape of the bSSFP profile remains unchanged. The additional  $e^{-i\vartheta}$  term contributes to the same rotation of all the data points around the origin of the complex plane. Therefore, the difference between Eq. (6) and (7) is only noticeable if  $\vartheta$  is sampled by different TR values (see Eq. 5) or if more than one tissue type with different  $\vartheta$  values is present. As a consequence, quantitative relaxometry, based on several bSSFP acquisitions with different RF phase increments  $\varphi$ , should not be affected by conjugating the phase evolution in Eq. (3), *as long as the tissue is pure*<sup>26</sup> that is well described by a single isochromat.

In the following section, it will be investigated whether this still holds, when the tissue of interest is composed of multiple signal components, each having a different accumulated phase  $\vartheta_i$ .

## 2.3 | Description of destructive interference in multi-component systems

A system of two components A and B and their magnetization  $m_A$  and  $m_B$  can be described using a single component bSSFP model<sup>2,9-12,15-19</sup> (or Eqs. 1, 3, 5) and the superposition principle<sup>20,27,28</sup>:

$$m_{\text{tot}}(t, \varphi) = m_A(t, \varphi) + m_B(t, \varphi). \quad (8)$$

Combining Eqs. (1), (3), and (8) and making use of (6) ( $\sigma = 0$ ) and (7) ( $\sigma = -1$ ), the total signal at  $TE = TR/2$

approximately becomes

$$m_{\text{tot}}(\text{TE}, \varphi) \approx 2ie^{i\psi} \cdot e^{i\varphi/2} \cdot \sum_{j \in \{A, B\}} e^{i\sigma\theta_j} \cdot f_j(\theta_j - \varphi) \cdot \sin \frac{\theta_j - \varphi}{2}. \quad (9)$$

As for the pure tissue, the functions  $f_j = \frac{a_j}{b_j + c_j \cos(\theta_j - \varphi)} e^{-\frac{\text{TE}}{T_{2j}}}$  can all be assumed to be real and positive. (Theory S3 contains a more detailed derivation of Eq. 9.) This expression enables a direct comparison between the different phase descriptions,  $\sigma = 0$  and  $\sigma = -1$ , and can be used to explain the presence or absence of destructive interference in multi-compartment systems. The terms  $e^{i\psi}$  and  $e^{i\varphi/2}$  are tissue independent and, thus, unaffected by the presence of multiple signal components.

Unlike pure tissues considered before, the outcome depends qualitatively on whether the correct ( $\sigma = 0$ ) phase description is used or not ( $\sigma = -1$ ):

- I. For  $\sigma = 0$ , the sum in Eq. (9) is real and the total phase can only take two opposed values:  $\psi + \varphi/2$ , if the sum is positive and  $\psi + \varphi/2 + \pi$  otherwise. Due to periodicity, the sum at any  $\varphi$  and  $\varphi + 2\pi$  must be of equal magnitude but of opposite sign. Therefore, there must be values of the RF phase increment  $\varphi$ , where the signal  $m_{\text{tot}}(\text{TE}, \varphi)$ , becomes zero. Note that this is not caused by banding artifacts associated with each component, but rather due to destructive interference. This cancellation must also be observable in more complex tissue compositions, consisting of three or more components.
- II. For  $\sigma = -1$ , the addends become complex due to the factors  $e^{-i\theta_j}$ , which will vary from component to component. Unlike the pure case, these factors can no longer be dragged out of the sum and absorbed in the global phase factor  $e^{i\psi}$  and are therefore observable: The sum will decompose into a real and imaginary component, each of which will exhibit destructive interference, but in general not for the same RF phase increment  $\varphi$ . Therefore, the magnitude of  $m_{\text{tot}}(\text{TE}, \varphi)$  cannot be expected to vanish for any  $\varphi$ . Also, the phase of  $m_{\text{tot}}(\text{TE}, \varphi)$  will show a more complicated behavior than the linear dependence on  $\varphi$ , which was obtained for  $\sigma = 0$ .

## 3 | METHODS

### 3.1 | Simulation experiments

The bSSFP profiles were simulated using MATLAB R2022a (The MathWorks Inc, Natick, MA) using Eqs. (1, 3, 5, 8), for both phase descriptions ( $\propto e^{i\frac{\text{TE}}{T_R}\theta}$ , corresponding to  $\sigma = 0$  in Eq. 9) and ( $\propto e^{-i\frac{\text{TE}}{T_R}\theta}$ , corresponding to  $\sigma = -1$

in Eq. 9) phase evolution, and for left and right coordinate handedness. Profiles were simulated for a 36%, 60% and 100% proton density acetone-water fraction, for different TR = [3.40, 3.62, 4.11, 4.62, 4.84, 5.14] ms with TE =  $\frac{\text{TR}}{2}$ . For simplicity  $T_1 = 3s$  and  $T_2 = 2.1s$  was assumed for both water and acetone. Additional parameters were  $B_0 = 2.89T$ ,  $\Delta B_0 = 0T$ ,  $\delta_{\text{cs,water}} = 0\text{ppm}$ ,  $\alpha = 35^\circ$  and 38 RF phase increment values  $\varphi = \frac{2\pi}{38}(k-1)$  for  $1 \leq k \leq 38$ . Based on experimental results, the relative chemical shift of acetone was fixed to  $-2.3\text{ ppm}$  and  $-2.5\text{ ppm}$  for the 60% and 36% acetone-water mixtures, respectively. For visual comparison the simulated profiles were rotated using the negative angle of the complex sum of the profiles.<sup>10</sup>  $\Delta B_0$  values and  $e^{i\psi}$  factors (Eqs. 1, 3, 5) were randomized to check profile shapes for invariances to  $\Delta B_0$  values and global phase factors.

To demonstrate that multi-compartment bSSFP profiles can be simulated using Bloch equations, additional numerical simulations were performed for 60% and 36% acetone-water mixtures (see Methods S1).

### 3.2 | MRI experiments in an acetone-water phantom at 3T

The bSSFP profiles were measured at 3T (MAGNETOM Prisma, Siemens Healthineers) using 18 phase-cycled bSSFP acquisitions with  $\varphi = \frac{2\pi}{18}(k-1)$  and  $1 \leq k \leq 18$ ,  $\alpha = 35^\circ$ , TR = [3.40, 3.62, 4.11, 4.62, 4.84, 5.14] ms, TE =  $\frac{\text{TR}}{2}$  and  $(1.5\text{ mm})^3$  isotropic resolution, in an acetone-water phantom, each contributing with their own distinct signal and phase behavior to the total measured bSSFP signal. The phantom contains 11 vials of 5 mL, each with a different acetone-water fraction, immersed in 2% agar. Acetone and water were mixed by recording the weight of the substances, which were then used to calculate proton densities, as described previously.<sup>29</sup>

Because data were acquired in a left-handed coordinate system,<sup>30,31</sup> bSSFP profiles were complex conjugated and then plotted in the (right-handed) complex plane to allow comparison with simulated data. To improve visual comparison, the bSSFP profiles were rotated using the negative angle of their complex sum before plotting.

### 3.3 | MRS experiments at 7T

Localized single voxel MRS was performed on the phantom vials containing  $f_{\text{PD}} = 36\%$  and  $f_{\text{PD}} = 60\%$  acetone to verify the chemical shifts. For MRS, a STEAM<sup>32</sup> sequence was used at 7T (MAGNETOM Terra, Siemens Healthineers) with a TR/TE/TM = 5s/20ms/13ms, 32 averages, a voxel of  $10 \times 10 \times 10\text{mm}^3$ , a spectral width of

5000 Hz and 4096 data points. Spectra were processed with JMRUI<sup>33</sup> and fitted using AMARES<sup>34</sup> to obtain the chemical shifts.

## 4 | RESULTS

### 4.1 | Simulation results

For single components, the elliptical shape of the bSSFP profile is independent of the phase definition of  $\sigma = 0$  and  $\sigma = -1$  and for randomized  $\Delta B_0$  values and global phase factors  $e^{i\psi}$  (Figure 1). Different  $e^{i\psi}$  factors led to a rotation of the profile in the complex plane. Note that this rotation is not visible because the profiles were rotated during post-processing. Changing the  $\Delta B_0$  values rotate the sampled points on the elliptical trajectories while leaving the trajectories themselves unchanged (Video S1).

Superposition was applied to obtain two-component profiles of water and acetone (Figure 2). For TR = 3.62 ms the phase difference of the water (Figure 2D) and ac-

tone (Figure 2E) profile was  $180^\circ$ , resulting in a combined profile that is symmetric, appearing as a single component profile.

Two-component simulations demonstrate that different phase definitions ( $\sigma = 0$  or  $\sigma = -1$ ) lead to significantly different profile shapes (Figures 3 and 4, Video S1), appearing either ribbon shaped, or heart-shaped. Complex conjugation leads to mirroring of the profile (Figures 3 and 4, column 1–4), which implies that a 60% acetone fraction profile with  $\sigma = 0$  (Figure 3F, dashed box) appears similar to a  $\sim 40\%$  acetone fraction profile that is complex conjugated (Figure 4G, dashed box).

For the  $\sigma = -1$  case, destructive interference was observed in 60% acetone for TR values close to 3.62 ms (Figure 3C,D), and in  $\sim 40\%$  acetone for TR = 4.84 ms (Figure S4 W, X). For other TR choices, the asymmetric profiles appear heart-shaped centered around the origin, without destructive interference (Figure 3 and 4, column 3–4), confirming theory.

For  $\sigma = 0$ , destructive interference is present for all TR values (Figures 3 and 4, column 1–2, Video S1), as expected according to theory.

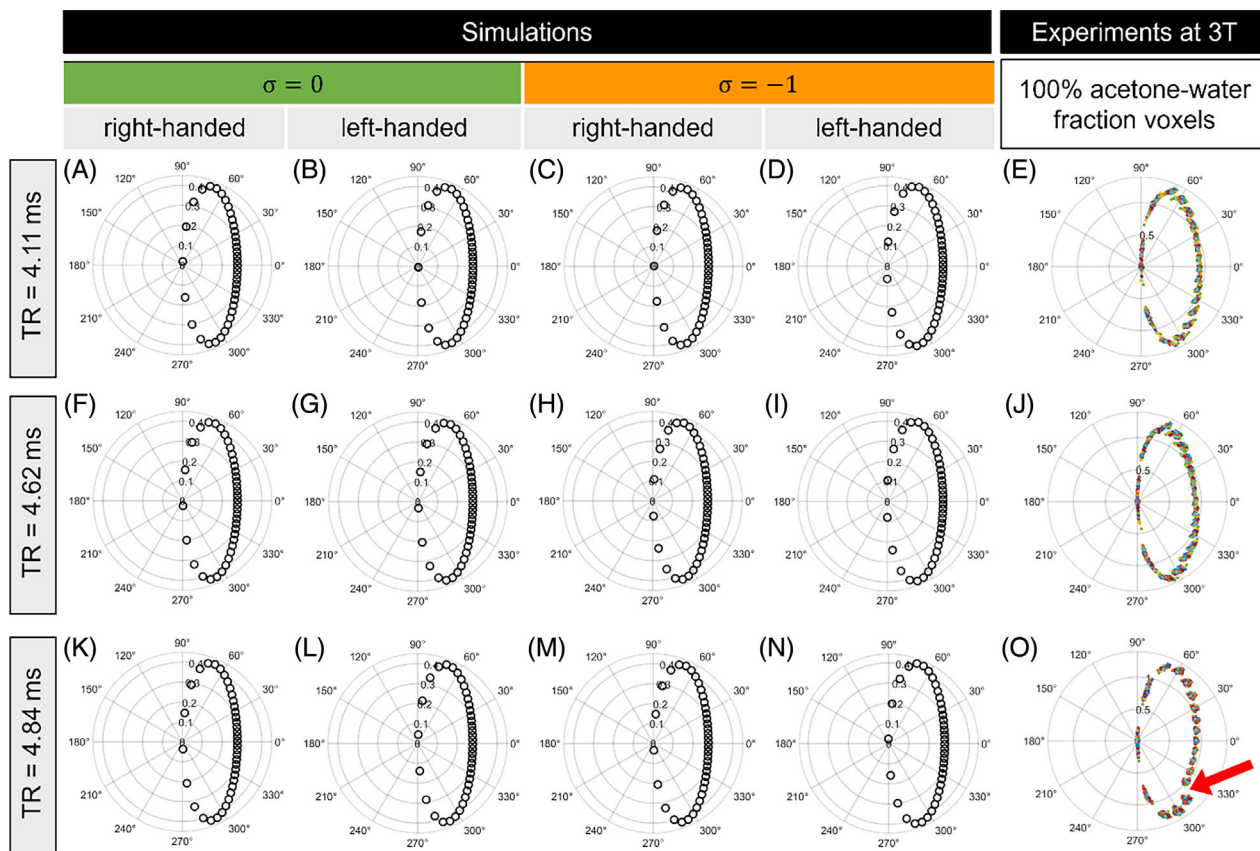


**FIGURE 1** Simulated and experimental steady-state free precession (bSSFP) signal profiles were obtained for a 100% acetone solution. All profiles remain elliptical for different repetition times. The red arrow indicates phase-drift (e.g.  $B_0$ -drift) effects. Banding is observed at the origin of the complex plots where the signal magnitude is near zero. The bSSFP signal profiles for all tested TR values are displayed in Figure S1.

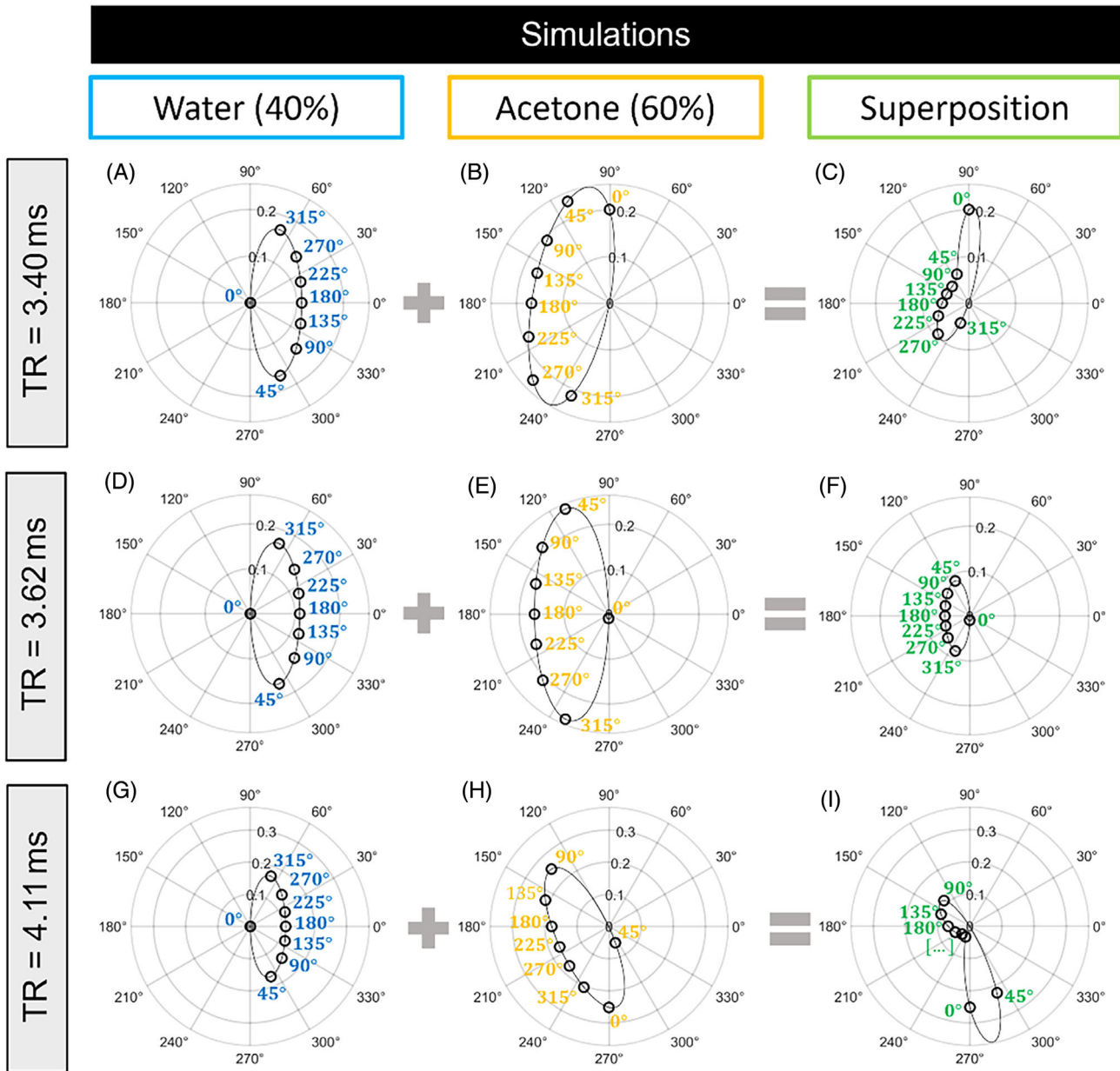


**FIGURE 2** Simulated bSSFP profiles for water (blue), acetone (yellow), and a 60% acetone-water mixture (green) using the correct phase sign case of  $\sigma = 0$ . Simulations were performed for different TR values. The RF phase increments are indicated in the plots in degrees ( $^{\circ}$ ). For TR = 3.62 ms, the acetone and water profiles are shifted 180 degrees, and the combined profile appears as a single component profile. Banding is observed at the origin of the complex plane of the single component profiles where the signal magnitude is near zero. Destructive interference is observed at the origin of the complex plane of the superimposed profile, where the signal magnitude is near zero. The bSSFP signal profiles for all tested TR values are displayed in Figure S2.

## 4.2 | MRI experiments

In the 100% acetone vial, mimicking a single-component system, the bSSFP profiles are symmetric and elliptical (Figure 1). In a few of these profiles, a gap can be observed within the ellipse, indicating phase-drift (Figures 10 and 30, red arrow).

In vials containing acetone-water fractions of 36% and 60%, the bSSFP profiles appear ribbon-shaped (Figure 3

and 4, last column) and are similar to profiles simulated using the  $\sigma = 0$  case. For this case, for every TR, the observed destructive interference matches predictions (Figure 3 and 4, column 1). In these experimental bSSFP profiles, the absence of destructive interference was never observed, which contradicts with the predicted profiles in the  $\sigma = -1$  case.

Interestingly, the bSSFP profiles obtained in the 60% fraction (Figure 3J) and the 36% fraction (Figure 4J),

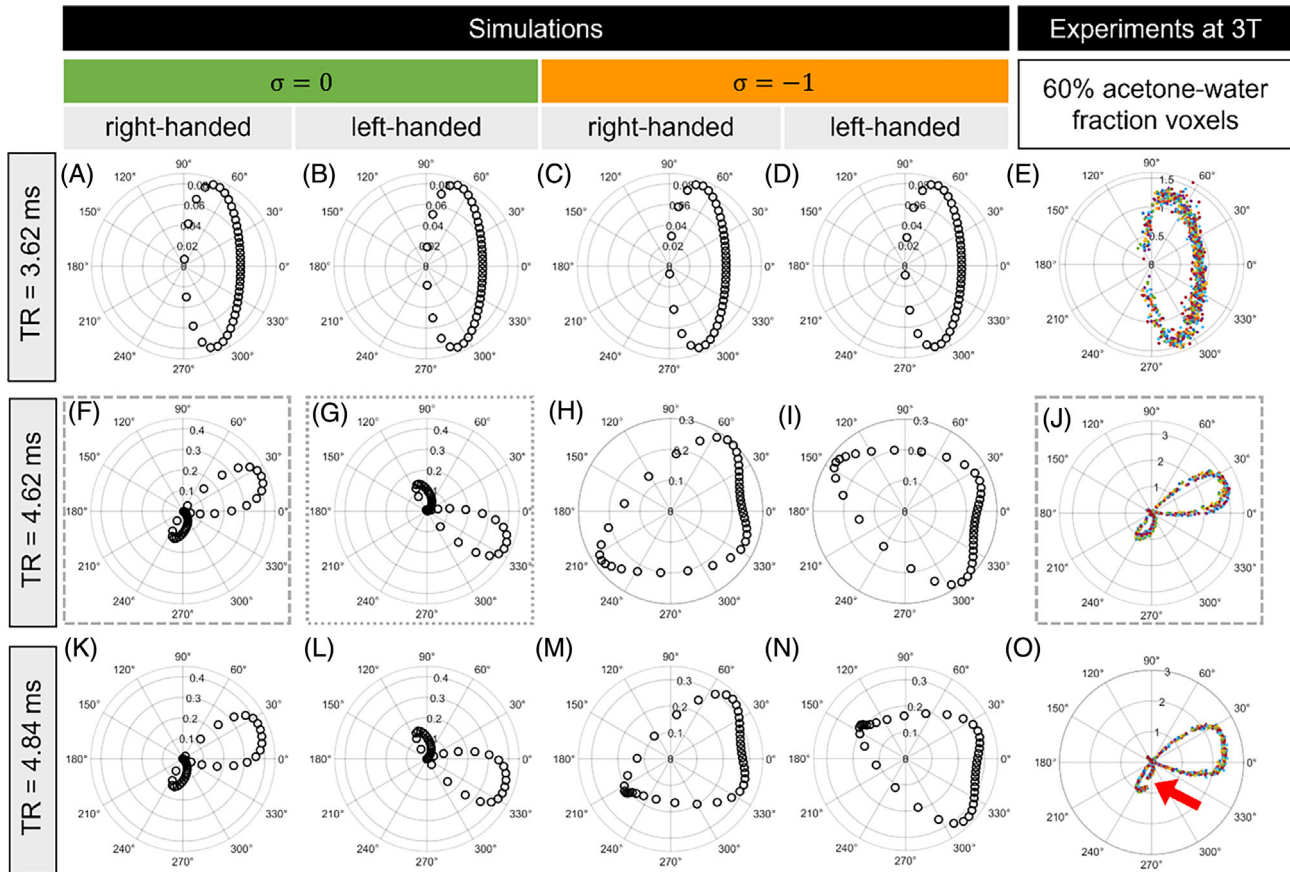


**FIGURE 3** Simulated and experimental bSSFP signal profiles obtained for a 60% acetone-water mixture. Simulated profiles appear differently depending on the phase description: The  $\sigma = 0$  case shows ribbon-shaped profiles while the  $\sigma = -1$  case shows heart-shaped profiles. Symmetric profiles appear when  $TR = 3.62$  ms, in this case, the two-component system appears as a single-component system. The dashed and dotted boxes indicate bSSFP profile shapes that appear mirrored for  $TR = 4.62$  ms. The red arrow indicates phase-drift effects. Destructive interference is observed at the origin of the complex plane where the signal magnitude is near zero. The bSSFP signal profiles for all tested  $TR$  values are displayed in Figure S3.

appear similar but mirrored from one another. These results show that knowledge of the coordinate handedness is mandatory for a correct evaluation of tissue fractions based on experimental bSSFP profiles (Figures 3 and 4, dashed and dotted boxes).

The chemical shift difference of acetone and water, measured with MRS, was  $-2.32 \pm 0.09$  ppm for the 60% and  $-2.48 \pm 0.09$  ppm for the 36% acetone mixtures (Figure 5).

Bloch simulations can also be used to simulate profiles coherent with the  $\sigma = 0$  case (Figure S5).

## 5 | DISCUSSION

This work demonstrated the importance of correct phase descriptions (referring to  $\sigma = 0$  in Eq. 9) for bSSFP profiles in multi-compartment systems, which was shown theoretically and confirmed by simulations and experiments.

In contrast to symmetric profiles, which are typically observed in systems with a single signal component, an incorrect phase description can lead to erroneous predictions of asymmetric profiles for systems with multiple signal components, which was tested and validated using acetone-water mixtures. Furthermore, to quantify component fractions correctly, knowledge about coordinate handedness of the data acquisition, which typically depends on the vendor, is crucial.

In single-component systems, using either phase description does not affect the bSSFP profile shapes, because such profiles are not subject to superposition and are thus symmetric. The shape is not affected by the changing coordinate handedness. These observations agree with the different phase descriptions reported in prior work.<sup>2,9-12,15-18</sup> Nevertheless, although the shape of the bSSFP profile remains unaffected, the data points could be arranged clockwise or counterclockwise, which can affect certain  $T_1$  and  $T_2$  quantification methods.<sup>9</sup>

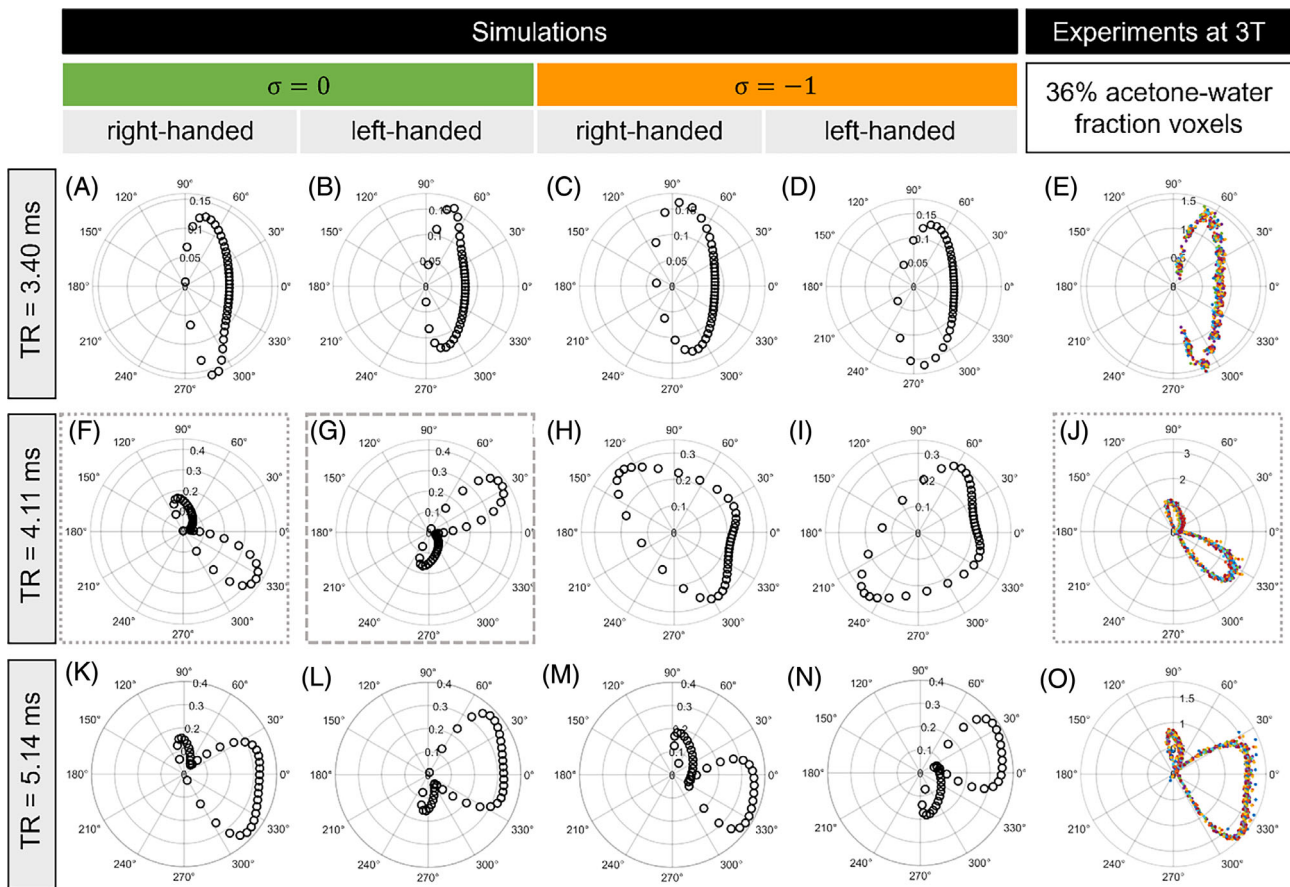


**FIGURE 4** Simulated and experimental bSSFP signal profiles obtained for a 36% acetone-water mixture. Simulated profiles appear differently depending on the phase description: The  $\sigma = 0$  case shows ribbon-shaped profiles while the  $\sigma = -1$  case shows heart-shaped profiles. Profiles are nearly symmetric when  $TR = 3.40$  ms. The dashed and dotted boxes indicate the mirrored profile shapes. Destructive interference is observed at the origin of the complex plane where the signal magnitude is near zero. The bSSFP signal profiles for all tested  $TR$  values are displayed in Figure S4.

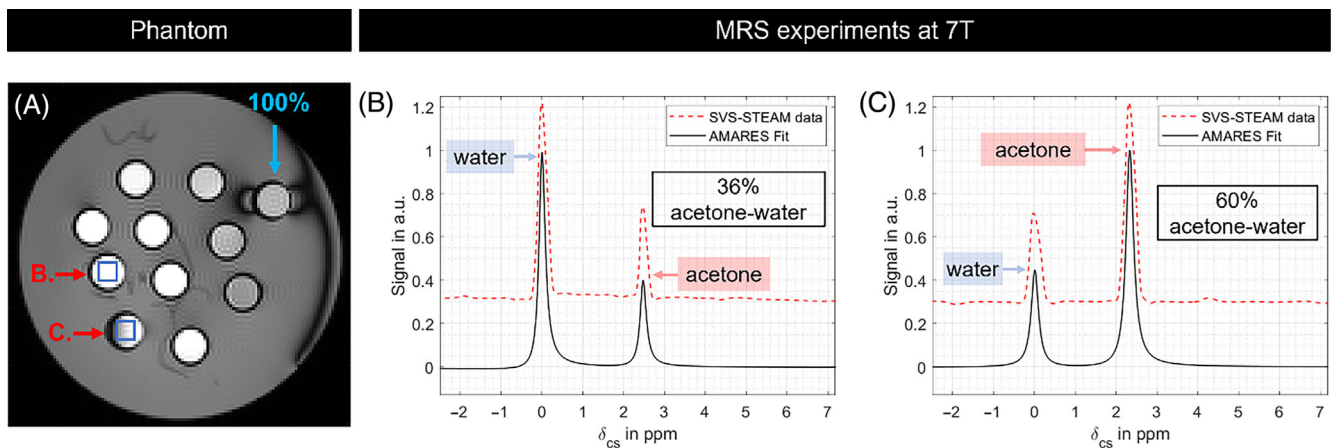


**FIGURE 5** (A) Acetone phantom of different vials for different acetone-water mixtures for an RF phase increment of  $180^\circ$ . The blue arrow indicates the 100% acetone vial, while the red arrows indicate images B and C. (B, C) Localized MRS performed at 7T in the vials containing a 36% and 60% proton density acetone-water fraction. The relative chemical shift of acetone is concentration dependent and was determined to be  $-2.48$  ppm for 36% and  $-2.32$  ppm for the 60% proton density acetone fraction relative to the chemical shift of water.



However, for two-compartment systems, there is a clear correct ( $\sigma = 0$ ) and incorrect ( $\sigma = -1$ ) way to combine the steady-state signals and subsequent phase evolution. The combination of two single-component profiles, using superposition, leads to significantly different bSSFP profile shapes depending on the chosen phase description in Eq. (9). For the case where  $\sigma = 0$ , destructive interferences were consistently observed, and for the case  $\sigma = -1$ , they were mostly absent. Therefore, being inconsistent with the phase leads to wrong bSSFP profile shapes and is therefore likely to cause systematic errors.

In addition, the choice of the coordinate handedness affects the “chirality” of the predicted profile, which is crucial for the correct estimation of tissue fractions. The use of right- or left-handed coordinate systems is not interchangeable because it causes a mirroring of the asymmetric profile and therefore corresponds to a different acetone-water fraction. In essence, this could be viewed as multiplying the underlying chemical shifts with  $-1$ , or as a straightforward tissue swap. For example, a complex conjugated profile of a 60% acetone-water fraction corresponds to a non-complex conjugated profile of a 40% acetone-water fraction.

The aforementioned emphasizes that the bSSFP signal equation relies on the difference between accumulated phase and RF phase increment denoted as  $\vartheta - \varphi$ . Altering the absolute sign of  $\vartheta$  may cause a tissue swap in multi-compartment models, while changing the absolute sign of  $\varphi$  results in a reversed identification of negative and positive bSSFP Fourier modes.

The current work aimed to describe analytically the bSSFP signal in multi-compartment systems. Numerical simulations of the Bloch equations reveal similar multi-compartment signal behavior of the  $\sigma = 0$  case (Methods S1). This demonstrates that different simulation frameworks can be used to generate reproducible results to describe multi-compartment bSSFP systems.<sup>14,27,28</sup>

In experimental data, the bSSFP profiles of 60% acetone-water appear as single component profiles for  $TR = 3.62$  ms. This is expected because, for certain  $TR$  values and chemical shifts, the individual bSSFP profiles of the two components may be shifted by  $180^\circ$  or  $0^\circ$  relative to each other, leading to two-component profiles which are visually perceived as elliptical single-component profiles. Therefore, it would be possible to estimate the chemical shift difference between water and acetone using bSSFP profile measurements. A rough chemical shift estimation based on bSSFP profiles agreed well with chemical shifts obtained with MRS. The observation that the chemical shift difference between acetone and water depends on the acetone-water fractions suggests that these types of mixtures are not well suited to validate

tissue fraction quantification techniques such as those performed with Dixon techniques,<sup>29,35</sup> unless verified with spectroscopy.

In summary, working with a consistent phase description ( $\sigma = 0$ ) is crucial to correctly describe multi-component and multi-compartment bSSFP profiles, specifically to avoid possible systematic errors in the analysis of bSSFP profile asymmetries for example at higher field strengths,<sup>26</sup> for  $T_1$  and  $T_2$  quantification in gray matter, white matter, and in muscles,<sup>9,11,20,21</sup> fat-water separation techniques<sup>4,5,36</sup> and fat quantification techniques using phase-cycled bSSFP.<sup>14</sup>

## 6 | CONCLUSIONS

The study demonstrates the vital importance of a consistent and correct treatment of phases in bSSFP signal descriptions of multi-compartment systems. The use of incorrect phase descriptions leads to erroneous bSSFP profiles as well as erroneous quantitative analysis of multi-compartment systems, which has been demonstrated both theoretically and experimentally.

## ACKNOWLEDGMENTS

This study was supported by funding received from the Swiss National Science Foundation, grant #PCEFP2\_194296. Open access funding provided by Universitat Bern.

## DATA AVAILABILITY STATEMENT

The acquired data are available for download in the following repository, <https://github.com/QIS-MRI/bSSFP-Getting-the-phase-consistent> with SHA-1 hash 7b2fb40c6bae636eeeadfebdadc2aaf4f9e7a4f7.

## ORCID

Nils M. J. Plähn  <https://orcid.org/0009-0002-2624-5412>

Roland Kreis  <https://orcid.org/0000-0002-8618-6875>

Carl Ganter  <https://orcid.org/0000-0002-6735-7448>

Jessica A. M. Bastiaansen  <https://orcid.org/0000-0002-5485-1308>

## REFERENCES

1. Bieri O, Scheffler K. Fundamentals of balanced steady state free precession MRI. *J Magn Reson Imaging*. 2013;38:2-11. doi:10.1002/jmri.24163
2. Zur Y, Stokar S, Bendel P. An analysis of fast imaging sequences with steady-state transverse magnetization refocusing. *Mag Res Med*. 1988;6:175-193. doi:10.1002/mrm.1910060206
3. Deoni SCL. Transverse relaxation time ( $T_2$ ) mapping in the brain with off-resonance correction using phase-cycled steady-state free precession imaging. *J Magn Reson Imaging*. 2009;30:411-417. doi:10.1002/jmri.21849

4. Vasanawala SS, Pauly JM, Nishimura DG. Linear combination steady-state free precession MRI. *Magn Reson Med.* 2000;43:82-90. doi:10.1002/(SICI)1522-2594(200001)43:1<82::AID-MRM10>3.0.CO;2-9
5. Çukur T, Bangertner NK, Nishimura DG. Enhanced spectral shaping in steady-state free precession imaging. *Magn Reson Med.* 2007;58:1216-1223. doi:10.1002/mrm.21413
6. Cukur T, Lustig M, Nishimura DG. Multiple-profile homogeneous image combination: application to phase-cycled SSFP and multicoil imaging. *Magn Reson Med.* 2008;60:732-738. doi:10.1002/mrm.21720
7. Hilbert T, Nguyen D, Thiran JP, Krueger G, Kober T, Bieri O. True constructive interference in the steady state (trueCISS). *Magn Reson Med.* 2018;79:1901-1910. doi:10.1002/mrm.26836
8. Hoff MN, Andre JB, Xiang Q. Combined geometric and algebraic solutions for removal of bSSFP banding artifacts with performance comparisons. *Magn Reson Med.* 2017;77:644-654. doi:10.1002/mrm.26150
9. Nguyen D, Bieri O. Motion-insensitive rapid configuration relaxometry. *Magn Reson Med.* 2017;78:518-526. doi:10.1002/mrm.26384
10. Shcherbakova Y, van den Berg CAT, Moonen CTW, Bartels LW. PLANET: an ellipse fitting approach for simultaneous  $T_1$  and  $T_2$  mapping using phase-cycled balanced steady-state free precession. *Magn Reson Med.* 2018;79:711-722. doi:10.1002/mrm.26717
11. Shcherbakova Y, van den Berg CAT, Moonen CTW, Bartels LW. On the accuracy and precision of PLANET for multiparametric MRI using phase-cycled bSSFP imaging. *Magn Reson Med.* 2019;81:1534-1552. doi:10.1002/mrm.27491
12. Shcherbakova Y, van den Berg CAT, Moonen CTW, Bartels LW. Investigation of the influence of  $B_0$  drift on the performance of the PLANET method and an algorithm for drift correction. *Magn Reson Med.* 2019;82:1725-1740. doi:10.1002/mrm.27860
13. Keskin K, Yılmaz U, Çukur T. Constrained ellipse fitting for efficient parameter mapping with phase-cycled bSSFP MRI. *IEEE Trans Med Imaging.* 2022;41:14-26. doi:10.1109/TMI.2021.3102852
14. Rossi GMC, Mackowiak ALC, Açıköz BC, et al. SPARCQ: a new approach for fat fraction mapping using asymmetries in the phase-cycled balanced SSFP signal profile. *Mag Res Med.* 2023;90:2348-2361. doi:10.1002/mrm.29813
15. Freeman R, Hill HDW. Phase and intensity anomalies in fourier transform NMR. *J Magn Reson.* 1969;4:366-383. doi:10.1016/0022-2364(71)90047-3
16. Lauzon ML, Frayne R. Analytical characterization of RF phase-cycled balanced steady-state free precession. *Concepts Magn Reson.* 2009;34A:133-143. doi:10.1002/cmr.a.20138
17. Ganter C. Steady state of gradient echo sequences with radiofrequency phase cycling: analytical solution, contrast enhancement with partial spoiling. *Magn Reson Med.* 2006;55:98-107. doi:10.1002/mrm.20736
18. Xiang QS, Hoff MN. Banding artifact removal for bSSFP imaging with an elliptical signal model: banding artifact removal for bSSFP imaging. *Magn Reson Med.* 2014;71:927-933. doi:10.1002/mrm.25098
19. Ernst RR, Anderson WA. Application of Fourier transform spectroscopy to magnetic resonance. *Rev Sci Instru.* 1966;37:93-102. doi:10.1063/1.1719961
20. Miller KL. Asymmetries of the balanced SSFP profile. Part I: theory and observation: balanced SSFP asymmetry: theory. *Magn Reson Med.* 2010;63:385-395. doi:10.1002/mrm.22212
21. Miller KL, Smith SM, Jezzard P. Asymmetries of the balanced SSFP profile. Part II: white matter. *Magn Reson Med.* 2010;63:396-406. doi:10.1002/mrm.22249
22. Bloch F. Nuclear induction. *Phys Rev.* 1946;70:460-474. doi:10.1103/Physrev.70.460
23. Tiesinga E, Mohr P, Newell D, Taylor B. CODATA Recommended Values of the Fundamental Physical Constants. 2018 <https://physics.nist.gov/cgi-bin/cuu/Value?gammabar>, <https://physics.nist.gov/cgi-bin/cuu/Value?gammabar>
24. Ernst RR, Bodenhausen G, Wokaun A. *Principles of Nuclear Magnetic Resonance in One and Two Dimensions.* Clarendon Press; 1990.
25. Scheffler K, Hennig J. Is TrueFISP a gradient-echo or a spin-echo sequence? *Magn Reson Med.* 2003;49:395-397. doi:10.1002/mrm.10351
26. Schäper J, Bauman G, Ganter C, Bieri O. Pure balanced steady-state free precession imaging (pure bSSFP). *Mag Res Med.* 2022;87:1886-1893. doi:10.1002/mrm.29086
27. Zhang S, Liu Z, Grant A, Keupp J, Lenkinski RE, Vinogradov E. Balanced steady-state free precession (bSSFP) from an effective field perspective: application to the detection of chemical exchange (bSSFPX). *J Magn Reson.* 2017;275:55-67. doi:10.1016/j.jmr.2016.12.002
28. Malik SJ, Teixeira RPAG, Hajnal JV. Extended phase graph formalism for systems with magnetization transfer and exchange. *Magn Reson Med.* 2018;80:767-779. doi:10.1002/mrm.27040
29. Reeder SB, Hines CD, Yu H, McKenzie CA, Brittain JH. On the definition of fat-fraction for in vivo fat quantification with magnetic resonance imaging. In Proceedings of the International Society for Magnetic Resonance in Medicine; 17. Honolulu, USA; 2009:211.
30. Haller S, Haacke EM, Thurnher MM, Barkhof F. Susceptibility-weighted imaging: technical essentials and clinical neurologic applications. *Radiology.* 2021;299:3-26. doi:10.1148/radiol.2021203071
31. Halefoglul AM, Yousem DM. Susceptibility weighted imaging: clinical applications and future directions. *WJR.* 2018;10:30-45. doi:10.4329/wjr.v10.i4.30
32. Frahm J, Merboldt KD, Hänicke W. Localized proton spectroscopy using stimulated echoes. *J Magn Reson (1969).* 1987;72:502-508. doi:10.1016/0022-2364(87)90154-5
33. Stefan D, Cesare FD, Andrasescu A, et al. Quantitation of magnetic resonance spectroscopy signals: the jMRUI software package. *Meas Sci Technol.* 2009;20:104035. doi:10.1088/0957-0233/20/10/104035
34. Vanhamme L, Van Den Boogaart A, Van Huffel S. Improved method for accurate and efficient quantification of MRS data with use of prior knowledge. *J Magn Reson.* 1997;129:35-43. doi:10.1006/jmre.1997.1244
35. Yu H, McKenzie CA, Shimakawa A, et al. Multiecho reconstruction for simultaneous water-fat decomposition and  $T_2^*$  estimation. *J Magn Reson Imaging.* 2007;26:1153-1161. doi:10.1002/jmri.21090
36. Cukur T, Nishimura DG. Fat-water separation with alternating repetition time balanced SSFP. *Magn Reson Med.* 2008;60:479-484. doi:10.1002/mrm.21692

## SUPPORTING INFORMATION

Additional supporting information may be found in the online version of the article at the publisher's website.

**Theory S1.** Contains a more detailed derivation of Equation (6) with more additional explanation.

**Theory S2.** Contains a more detailed derivation of Equation (7) with more additional explanation.

**Theory S3.** Contains a more detailed derivation of Equation (9) with more additional explanation.

**Methods S1.** Contains a theory and method section for performing Bloch simulations for simulating acetone-water bSSFP profiles.

**Figure S1.** Contains the 100% acetone bSSFP profiles for all tested TR values in simulations and experiments.

**Figure S2.** Illustrates the superposition principle for 40% water bSSFP profiles and 60% acetone bSSFP profiles for all tested TR values for  $\sigma = 0$  simulations.

**Figure S3.** Contains the 60% acetone-water bSSFP profiles for all tested TR values in simulations and experiments.

**Figure S4.** Contains the 36% acetone-water bSSFP profiles for all tested TR values in simulations and experiments.

**Figure S5.** Compares the 36% and 60% acetone-water bSSFP profiles simulated via Bloch simulations and analytical model simulations for  $\sigma = 0$ .

**Video S1.** Animation of the impact of TR and choice of phase description on the bSSFP profile shape in a one- and two-component phantom, which contains water and acetone. *One signal component:* For both phase descriptions the data points are sorted counterclockwise for  $k = 1$  to 6

for increasing RF phase increments  $\varphi_k$  along the elliptical trajectory. When the correct phase description is used ( $\sigma = 0$ , black circles), the data points show an approximately constant phase with  $\psi + \frac{\varphi_k}{2} \pm \frac{\pi}{2}$  independent of TR (see Section 2.3, Equation [9]). When the incorrect phase description is used ( $\sigma = -1$ , red triangles) the data points do not exhibit constant phases concerning a constant RF phase increment  $\varphi_k$ . For both phase descriptions the elliptical trajectory remains the same. *Two signal components:* For both phase descriptions the data points are sorted counter-clockwise for  $k = 1$  to 6 for increasing RF phase increments  $\varphi_k$  along the elliptical trajectory. When the correct phase description is used ( $\sigma = 0$ , black circles), the data points show an approximately constant phase with  $\psi + \frac{\varphi_k}{2} \pm \frac{\pi}{2}$  independent of TR (see Section 2.3, Equation [9]). When the incorrect phase description is used ( $\sigma = -1$ , red triangles) the data points do not exhibit constant phases concerning a constant RF phase increment  $\varphi_k$ . Using a different phase description leads to significantly different trajectories of the bSSFP profiles in the complex plane.

**How to cite this article:** Plähn NMJ, Poli S, Peper ES, et al. Getting the phase consistent: The importance of phase description in balanced steady-state free precession MRI of multi-compartment systems. *Magn Reson Med.* 2024;1-11. doi: 10.1002/mrm.30033